

---

# Learning to Mask and Permute Visual Tokens for Vision Transformer Pre-Training

---

Lorenzo Baraldi<sup>1\*</sup>   Roberto Amoroso<sup>2\*</sup>   Marcella Cornia<sup>2</sup>   Lorenzo Baraldi<sup>2</sup>  
Andrea Pilzer<sup>3</sup>   Rita Cucchiara<sup>2,4</sup>

<sup>1</sup>University of Pisa, Italy   <sup>2</sup>University of Modena and Reggio Emilia, Italy

<sup>3</sup>NVIDIA AI Technology Center, Italy   <sup>4</sup>IIT-CNR, Italy

## Abstract

The use of self-supervised pre-training has emerged as a promising approach to enhance the performance of visual tasks such as image classification. In this context, recent approaches have employed the Masked Image Modeling paradigm, which pre-trains a backbone by reconstructing visual tokens associated with randomly masked image patches. This masking approach, however, introduces noise into the input data during pre-training, leading to discrepancies that can impair performance during the fine-tuning phase. Furthermore, input masking neglects the dependencies between corrupted patches, increasing the inconsistencies observed in downstream fine-tuning tasks. To overcome these issues, we propose a new self-supervised pre-training approach, named Masked and Permuted Vision Transformer (MaPeT), that employs autoregressive and permuted predictions to capture intra-patch dependencies. In addition, MaPeT employs auxiliary positional information to reduce the disparity between the pre-training and fine-tuning phases. In our experiments, we employ a fair setting to ensure reliable and meaningful comparisons and conduct investigations on multiple visual tokenizers, including our proposed  $k$ -CLIP which directly employs discretized CLIP features. Our results demonstrate that MaPeT achieves competitive performance on ImageNet, compared to baselines and competitors under the same model setting. Source code and trained models are publicly available at: <https://github.com/aimagelab/MaPeT>.

## 1 Introduction

Self-supervised pre-training models have achieved remarkable success in boosting the performance of Transformer-based architectures in Computer Vision. Inspired by the BERT model [11], the Masked Image Modeling (MIM) pre-training objective [1] has become widely adopted in literature as a powerful self-supervision method for vision tasks. In particular, this pre-training objective involves masking random image patches and reconstructing the corrupted visual input. While several recent studies have refined the MIM approach [7, 15, 19], there has been little exploration of alternative pre-training objectives in the visual domain. In contrast, in the field of Natural Language Processing (NLP), several methods [33, 38] have surmounted the BERT pre-training objective with the introduction of different paradigms that aim to solve the drawbacks of previous methods.

Drawing inspiration from NLP, we investigate a permutation-based pre-training strategy, which we term Permuted Image Modeling (PIM). This approach autoregressively predicts permuted image patches maintaining contextual bi-directionality without corrupting any part of the input. Despite offering an improvement over the standard MIM-based objective, the autoregressive technique of PIM reduces the amount of positional information available for each prediction. To tackle this issue, we propose a Masked and Permuted pre-training solution for Vision Transformers (MaPeT) which

---

\*Equal contribution. E-mail: [lorenzo.baraldi@phd.unipi.it](mailto:lorenzo.baraldi@phd.unipi.it), [roberto.amoroso@unimore.it](mailto:roberto.amoroso@unimore.it).

leverages auxiliary position information as input during pre-training, thereby allowing the model to access the positional information of every image patch.

In addition to the pre-training objective, a crucial aspect of self-supervised vision pre-training is the design of visual targets, used as supervisory signal. While some works have employed low-level and hand-crafted visual features [22, 25, 35], the dominant approach is to employ discrete visual tokens to reconstruct the corrupted visual input [1, 7, 15, 30]. In this context, although BEiT [1] initially employed DALL-E [32] visual tokens, its performance has been surpassed by VQ-KD, proposed in BEiT v2 [30]. In particular, VQ-KD employs an encoder-decoder architecture that reconstructs CLIP semantic features and is directly trained on ImageNet-1k [10], requiring retraining to achieve satisfactory results on other datasets. In contrast to previous works, we propose  $k$ -CLIP, a novel discrete tokenizer for generating visual tokens that can directly employ CLIP features without requiring training an ad hoc discrete autoencoder.

To evaluate the effectiveness of the proposed pre-training model and tokenizer, we conduct experiments that provide a fair comparison between models, adhering to the same experimental settings. This approach allows to accurately measure the efficacy of each model under consistent conditions and effectively compare their relative strengths and weaknesses. Experimental results demonstrate that our MaPeT model achieves competitive performance and surpasses both mask- and permutation-based image pre-training. Additionally, we show that the visual tokens extracted by our proposed  $k$ -CLIP tokenizer exhibit richer semantic information than competitors, outperforming both DALL-E and VQ-KD visual tokens when employed directly for image classification.

## 2 Related Work

**Self-supervised learning.** Several solutions have been introduced in the last years to effectively pre-train vision-based architectures via self-supervised learning, initially based on different pretext tasks [12, 17, 28, 34, 39] and then exploiting contrastive learning paradigms [6, 8, 18, 20, 29]. The advent of Vision Transformer models (ViT) [14] has pushed towards the introduction of new increasingly sophisticated self-supervised pre-training strategies [1, 4, 5, 9]. In this context, motivated by the great success in NLP, some attempts have been made to effectively adapt the Masked Language Modeling paradigm [11, 24] and its auto-regressive variant [3] in the Computer Vision domain, either by directly predicting pixels [5], image patches [14], or discrete visual tokens [1]. In particular, the recently proposed BEiT approach [1] effectively performs pre-training via image patch masking and predicts the discretized labels [32] of masked patches. Since the introduction of BEiT, many subsequent methods based on similar pre-training strategies have been presented [7, 13, 15, 19, 35–37]. Some of these methods [7, 15, 19] have introduced an encoder-decoder architecture to separate uncorrupted encoded information from masked tokens, which are employed directly as input to the decoder. Inspired by findings from NLP literature [33, 38], our proposed method aims to overcome the limitations of Masked Image Modeling in self-supervised pre-training.

**Visual targets.** In the domain of self-supervised learning, visual targets are a set of specific objectives that are used as the supervisory signal to pre-train visual models. Based on the type of signal, the targets can be categorized into low-level visual features, hand-crafted features, and visual tokens. Some recent studies [16, 19, 22, 25, 37] have utilized pixel information as the low-level supervisory signal for self-supervised pre-training. In contrast, [35] have used HOG hand-crafted features to reconstruct the masked visual input. More recently, visual targets based on CLIP [31] have been utilized with remarkable success, either by directly employing CLIP features [21, 36, 40] or training a discrete tokenizer [30] to reconstruct the semantic features encoded by CLIP. In our method, we propose a discrete visual tokenizer based on CLIP features which offers a novel approach to visual pre-training without the need for specific training over a particular dataset.

## 3 Preliminaries

In this section, we detail two pre-training strategies that are the starting point of our proposal, *i.e.*, Masked Image Modeling (MIM) and Permuted Image Modeling (PIM), and we introduce the terminology used in the rest of the paper.

**Image patches.** In this study, we adopt ViT [14] as the backbone network for our architecture. ViT splits an image into a sequence of 2D image patches, which are linearly projected to the

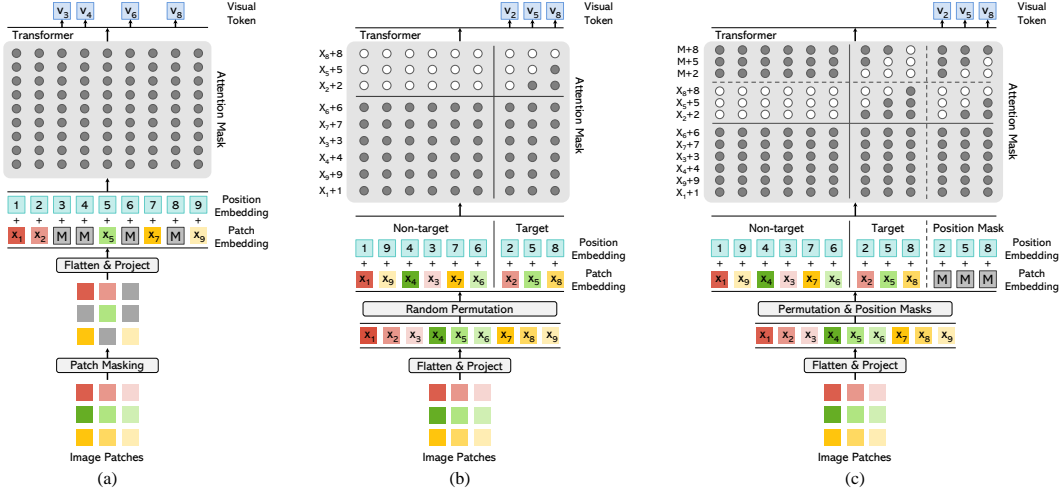


Figure 1: (a) Masked Image Modeling (MIM). (b) Permuted Image Modeling (PIM). (c) Masked and Permuted pre-training for Vision Transformers (MaPeT). While MIM reconstructs visual tokens from randomly masked image patches, PIM autoregressively predicts tokens associated with permuted image patches. MaPeT uses PIM to capture intra-patch dependency and takes auxiliary position information as input to ensure that the model sees a full sequence of patches at each target position.

model embedding space and elaborated through multiple attention blocks. Given an input image  $x \in \mathbb{R}^{H \times W \times C}$ , this is mapped into a sequence of  $N$  square patches  $\{x_i^p\}_{i=1}^N$ , where  $x_i^p \in \mathbb{R}^{P \times P \times C}$  is the  $i$ -th patch of the input image. Subsequently, a linear layer is applied to each flattened patch to project it to the input dimensionality of the model  $D$ , outputting the patch embeddings  $\{x_i\}_{i=1}^N$ , where  $x_i \in \mathbb{R}^D$ , which are then added to the learnable 1D positional embeddings  $E_{\text{pos}} \in \mathbb{R}^{N \times D}$ .

The ViT [14] encoder consists of  $L$  identical layers of Transformer blocks, where the output embeddings of the last layer represent the encoded representations of the  $N$  input image patches. In our experiments, we consider an image dimension of  $224 \times 224$  with a patch dimension  $P$  of  $16 \times 16$ , constituting an input sequence of  $14 \times 14 = 196$  patch embeddings.

**Visual tokens.** In self-supervised pre-training, learned supervisory signals are typically used to effectively pre-train the visual backbone. In this work, we employ visual tokens as supervisory signals during the pre-training phase. Specifically, we represent targets as a discrete token sequence, accomplished by utilizing a visual tokenizer  $\mathcal{T}(x)$  on the input image  $x$ . The visual tokenizer maps the image pixels onto a visual codebook (or vocabulary), generating a sequence of tokens  $v = [v_1, \dots, v_N] \in \mathcal{V}^{(H/P) \times (W/P)}$ , where  $\mathcal{V}$  represents the vocabulary containing discrete token indices. Our approach employs a  $14 \times 14$  grid of visual tokens to represent each image, while the vocabulary size is set to  $|\mathcal{V}| = 8192$ .

**Masked Image Modeling (MIM).** Inspired by the Masked Language Modeling strategy utilized in BERT [11], the MIM paradigm is a pre-training technique for vision tasks that aims to recover visual information from a corrupted input image. This is achieved by randomly masking a portion of the image patches and predicting the visual tokens related to the corrupted region of the input, as depicted in Fig. 1 (a). Like Masked Language Modeling, MIM has some inherent disadvantages. Firstly, a mask token  $M$  is introduced during pre-training and never used during fine-tuning, leading to a discrepancy in the pre-training and fine-tuning phases. Secondly, given the masked tokens  $\bar{x}$  and the uncorrupted context  $\tilde{x}$ , the probability  $p(\bar{x} | \tilde{x})$  is typically factorized, assuming the independence of reconstructed patches. To address these issues, the NLP literature has investigated a permutation-based variant [38] that can reduce the disadvantages of standard Masked Language Modeling. These results motivate us to investigate the application of this strategy to vision tasks.

**Permuted Image Modeling (PIM).** The PIM self-supervised pre-training objective differs from MIM in two key components: the use of patch permutations and attention masking to capture bidirectional contexts. Specifically, PIM permutes patch embeddings, splits them into non-target and target patches, and predicts the visual tokens associated with the target patches using an auto-regressive approach. Attention masking is then applied to reduce the visibility of patches in the attention process, allowing a target patch to not access its contextual information (*i.e.*, its content) during prediction while

remaining visible to patches that come after it in the permuted order. A visual representation of the process is shown in Fig. 1 (b).

Formally, given an input image  $\mathbf{x}$ , we extract the patch embeddings  $\{\mathbf{x}_i\}_{i=1}^N$ , and tokenize it into  $N$  visual tokens  $\{v_i\}_{i=1}^N$ . We define  $\mathcal{Z}_t$  as the set of all  $N!$  possible permutations of the length- $N$  index sequence  $\{1, 2, \dots, N\}$ . Given a permutation  $\mathbf{z}$ , we use  $z_t$  and  $\mathbf{z}_{<t}$  to denote the  $t$ -th element and the first  $t - 1$  elements of  $\mathbf{z}$ , respectively. After applying  $\mathbf{z}$ , the permuted patch embeddings are fed into an  $L$ -layer ViT backbone to extract the final hidden representations. For each input embedding  $\mathbf{x}_{z_t}$  at position  $z_t$  in the considered permutation  $\mathbf{z}$ , we use a softmax classifier to predict the corresponding visual token. The goal of PIM is to maximize the following log-likelihood objective:

$$\max_{\theta} \sum_{\mathbf{x} \in \mathcal{D}} \mathbb{E}_{\mathbf{z} \in \mathcal{Z}_t} \left[ \sum_{t=c+1}^N \log p_{\theta}(v_{z_t} | \mathbf{x}_{z_{<t}}) \right], \quad (1)$$

where  $\theta$  represents the model parameters,  $\mathcal{D}$  denotes the training dataset,  $\mathbf{x}_{z_{<t}}$  are the only patch embeddings that are visible at position  $z_t$ , and  $c$  is a cutting point applied to split the permutation  $\mathbf{z}$  in a subset of non-target patch embeddings  $\mathbf{x}_{z_{<c}}$  and target patch embeddings  $\mathbf{x}_{z_{>c}}$ . The aim of  $c$  is to reduce the number of visual tokens to be predicted, thus mitigating optimization difficulties.

While MIM preserves full positional information of each image patch, during the prediction process, PIM can access the contextual and positional information only of the  $t - 1$  patches that precede  $z_t$ , as shown in Eq. 1. Given this lack of full positional information, PIM introduces an input discrepancy between pre-training and fine-tuning, underscoring the necessity for a pre-training technique that combines the advantages of both MIM and PIM while mitigating their respective limitations.

## 4 Proposed Method

In this section, we present MaPeT, a novel pre-training paradigm that combines masked and permuted image modeling strategies. In addition, we also introduce the  $k$ -CLIP visual tokenizer, which exploits discretized CLIP features to produce visual tokens.

### 4.1 Masked and Permuted Pre-Training for Vision Transformers

Drawing inspiration from NLP literature [33, 38], we propose a novel pre-training methodology called **M**asked and **P**ermuted **V**ision **T**ransformer (MaPeT) which builds on the strengths of both MIM and PIM to enhance performance on vision tasks. In particular, our approach overcomes the independence assumption of reconstructed patches, thus capturing intra-patch dependencies more effectively. Moreover, MaPeT incorporates auxiliary position embeddings during pre-training, enabling the model to access position information for all patches, thereby resolving the pre-training fine-tuning discrepancy introduced by PIM. Fig. 1 (c) shows an overview of the MaPeT approach.

Given a permutation  $\mathbf{z}$  and a cutting point  $c$ , MaPeT can predict the visual token associated with an input patch embedding  $\mathbf{x}_{z_t}$  by leveraging the content and position of the preceding  $\mathbf{x}_{z_{<t}}$ , as well as the position of the subsequent target embeddings  $\mathbf{x}_{z_{>t}}$ . To this end, we introduce the concept of learnable masked token  $M \in \mathbb{R}^D$ , which is used to express the positional information of  $\mathbf{x}_{z_{>c}}$ . By repeating  $N - c$  times the token  $M$ , we obtain  $\{M_i\}_{i=c+1}^N$  identical masked tokens, which are then summed to the positional embedding  $\{E_{\text{pos}}^i\}_{i=z_{c+1}}^{z_N}$  of each target  $\mathbf{x}_{z_{>c}}$ . These resulting position-aware masked tokens  $M_{\text{pos}} = \{M_{c+1} + E_{\text{pos}}^{z_{c+1}}, \dots, M_N + E_{\text{pos}}^{z_N}\}$  are concatenated to the input sequence of patch embeddings  $\mathbf{H}^0$  thus obtaining the augmented input  $\mathbf{H}_M^0 = [\mathbf{H}^0, M_{\text{pos}}]$ . Note that the positional embeddings are permuted according to the same permutation  $\mathbf{z}$  applied to the patches. For convenience, we introduce  $M_{z_{\geq t}}$  which represents the subset  $\{M_{\text{pos}}^i\}_{i=\max(1, t-c)}^{N-c}$ . Intuitively, when  $t \leq c$ , we have that  $M_{z_{\geq t}}$  comprises all  $M_{\text{pos}}$ . Conversely, when  $t > c$ ,  $M_{z_{\geq t}}$  only includes the position-aware masked tokens related to  $\mathbf{x}_{z_{\geq t}}$ .

The training objective of our MaPeT model is to maximize the log-likelihood of predicting the visual token  $v_{z_t}$  associated with the patch embedding  $\mathbf{x}_{z_t}$  given  $\mathbf{x}_{z_{<t}}$ :

$$\max_{\theta} \sum_{\mathbf{x} \in \mathcal{D}} \mathbb{E}_{\mathbf{z} \in \mathcal{Z}_t} \left[ \sum_{t=c+1}^N \log p_{\theta}(v_{z_t} | \mathbf{x}_{z_{<t}}, M_{z_{\geq t}}) \right]. \quad (2)$$

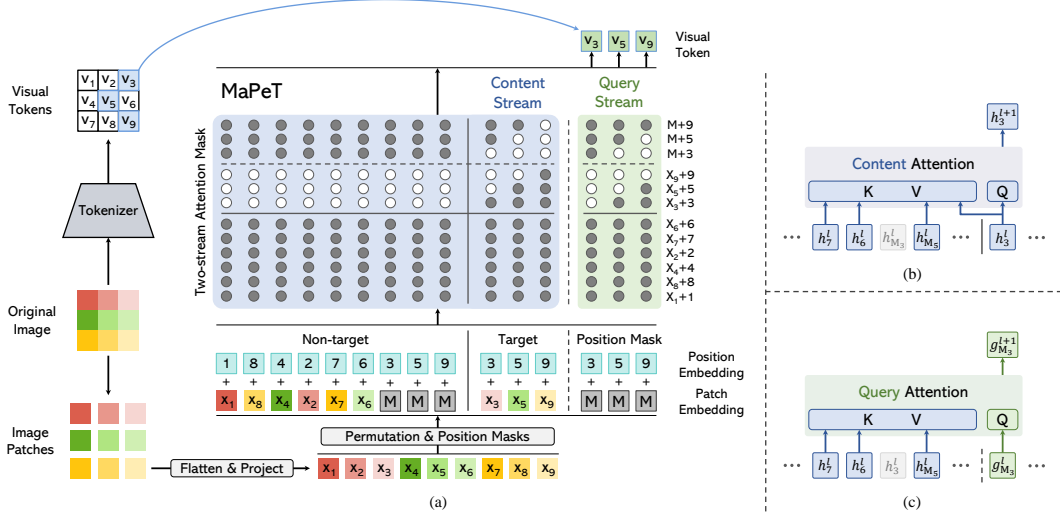


Figure 2: Overview of our MaPeT pre-training (a), with content stream attention (b), which follows the standard self-attention mechanism, and query stream attention (c), which lacks information about the content of the patch embedding  $x_{z_t}$  whose visual token  $v_{z_t}$  is to be predicted. The blue and green masks in (a) are the content and query attention masks employed in the two-stream self-attention.

By doing so, MaPeT allows the patch embedding  $x_{z_t}$  to attend to contextual information of the patch embeddings  $x_{z_{<t}}$  as well as the positional information of  $x_{z_{>t}}$ . This approach compensates for the position discrepancy of PIM and provides the model with information about the position of the target patches whose visual tokens are to be predicted. Fig. 2 shows an illustration of our MaPeT method.

**Two-stream self-attention pre-training.** Since the target patch embeddings  $x_{z_{>c}}$  follow the permuted order, the next predicted patch can occur in any position. As a consequence, masking the attention matrix of a ViT encoder, instead of corrupting the input like in MIM, makes the backbone architecture non-trivial. To implement PIM on a ViT backbone, we adopt the two-stream self-attention mechanism introduced by XLNet [38]. Specifically, our model consists of two attention streams: a query stream and a content stream. The query stream  $g_\theta(x_{z_{<t}}, M_{z_{>t}})$  accesses the content of the previous patches in the permuted sequence at a given position  $t$ . However, it does not access the content of  $x_{z_t}$ , only viewing the position  $M_{z_{>t}}$  of the subsequent patches. In contrast, the content stream  $h_\theta(x_{z_{<t}}, M_{z_{>t}})$  encodes the content of both the previous elements in the sequence and the element in position  $z_t$ , with positional information  $M_{z_{>t}}$  of the remaining patches. The input of the first query stream layer  $g^{(0)}$  consists of the masked elements  $M_{\text{pos}}$ , which encode the position of the target patch embeddings  $x_{z_{>c}}$ . Instead, the input of the first content stream layer  $h^{(0)}$  is the augmented input sequence  $H_M^0$ . Formally, for each Transformer layer  $l$  with  $l = 1, \dots, L$ , the attention mechanism of both content and query streams can be defined as follows:

$$\begin{aligned} h_{z_t}^{(l)} &\leftarrow \text{Attention}(Q = h_{z_t}^{(l-1)}, KV = (\mathbf{h}_{z_{\leq t}}^{(l-1)}, \mathbf{h}_{M_{z_{>t}}}^{(l-1)}); \theta), \\ g_{z_t}^{(l)} &\leftarrow \text{Attention}(Q = g_{z_t}^{(l-1)}, KV = (\mathbf{h}_{z_{<t}}^{(l-1)}, \mathbf{h}_{M_{z_{\geq t}}}^{(l-1)}); \theta), \end{aligned} \quad (3)$$

where  $Q$ ,  $K$ , and  $V$  are respectively queries, keys, and values of the attention operator. Both query and content streams use separate attention masks to limit the visible contextual and positional information for each patch. During pre-training, the output of the query stream is used as the model output. At the fine-tuning step, the query stream is dropped, and only the content stream is used, returning to the standard ViT backbone. Fig. 2 shows an illustration of the content stream (b), the query stream (c), and how they are integrated into our MaPeT architecture.

**Attention masking.** In order to limit the number of visible patches in the content and query attention operations, as described in Eq. 3, MaPeT leverages attention masking. In particular, the permutation  $z$  influences the creation of two distinct attention masks: one for the content attention stream and one for the query attention stream. The content mask guarantees that only patch embeddings  $x_{z_{<t}}$  and positional tokens  $M_{z_{>t}}$  are visible to the patch embedding  $x_{z_t}$  in the content stream. On the other hand, the query mask ensures that only patch embeddings  $x_{z_{<t}}$  and positional tokens  $M_{z_{\geq t}}$  are visible to  $x_{z_t}$  in the query stream.

## 4.2 $k$ -CLIP: Discretized CLIP-based Tokenizer

The role of visual tokenizers in pre-training pipelines is significant, as they provide crucial guidance for downstream fine-tuning outcomes. To possibly reduce the overhead of tokenizer retraining of previously proposed approaches [30], we explore the impact of directly utilizing discretized CLIP features. In particular, we propose a novel visual tokenizer, called  $k$ -CLIP, that employs discretized CLIP features as visual tokens. Our method does not rely on any pre-training or supervised data to create the visual tokens, thus enabling pre-training without access to large amounts of labeled data or a particular pre-training dataset. Furthermore, the use of CLIP features enables our method to capture high-level visual semantics that are more meaningful for downstream tasks, further improving the performance of the learned representations.

Specifically, we sample visual features from the ImageNet dataset [10] using the CLIP model [31] and cluster them using  $k$ -means to obtain  $|\mathcal{V}| = 8192$  centroids. During pre-training, these centroids are indexed to retrieve the corresponding visual tokens for prediction. Formally, our visual tokenizer  $\mathcal{T}(\mathbf{x})$  consists of a ResNet-based CLIP visual encoder and a  $k$ -means model. The visual encoder  $f_v : \mathbb{R}^{H \times W \times C} \rightarrow \mathbb{R}^{H_c \times W_c \times D_c}$  maps an input image  $\mathbf{x}$  to a grid of visual features that correspond to the activations produced by the last convolutional layer of the CLIP backbone. The visual features are then reshaped to a  $N_c \times D_c$  matrix, where  $N_c = H_c \times W_c$ . In our method, the CLIP visual encoder generates visual features of shape  $N_c \times D_c = 196 \times 4096$ , which are subsequently indexed by  $k$ -means and mapped to a sequence of 196 discrete visual tokens  $\mathbf{v} = [v_1, \dots, v_N] \in \mathcal{I}$ . The set of visual tokens  $\mathbf{v} = \{v_i\}_{i=1}^N$  is defined by the  $k$ -means centroid indexes  $\mathcal{I} = \{1, \dots, |\mathcal{V}|\}$ . To mitigate the computational complexity, we randomly sample 2% of the approximately 250 million  $D_c$ -dimensional CLIP features extracted from ImageNet. The sampled feature collection is then used to fit the  $k$ -means clustering model.

## 5 Experiments

### 5.1 Experimental Setup

Self-supervised pre-training literature has introduced several training and fine-tuning procedures that encompass different tokenizers, hyperparameters, and visual backbones. To ensure a fair and unbiased comparison among these pre-training algorithms, we opt to evaluate our MaPeT method, as well as the related approaches in the literature, using identical experimental configurations. This strategy allows for the isolation of the algorithmic factor in the experiments and promotes unbiased comparisons of pre-training objectives. In order to assess the effectiveness of the pre-trained objective under consideration, we fine-tune our models on a downstream classification task.

**Pre-training setup.** We first investigate the influence of the visual tokenizer, evaluating the proposed  $k$ -CLIP against VQ-KD [30]. To minimize the computational effort, we pre-process the ImageNet-1k training dataset [10] for both the tokenizers and store the visual tokens associated with each image. For this reason, our pre-training augmentation policy only includes color jittering to preserve image patch positions corresponding to the pre-extracted visual tokens.

We compare MaPeT against different pre-training objectives. In particular, we employ a ViT-based backbone that is pre-trained according to the pure MIM objective formulation. Note that this differs from the pre-training strategy proposed by the BEiT approach [1] as it lacks the block-wise masking algorithm, which progressively extracts multiple blocks of patches until 40% of the positions are masked. In our MIM-based pre-training, we replace the block-wise masking strategy with a random patch masking approach, thus keeping it similar to a BERT-like solution [11] applied to Computer Vision tasks. Analogously, we also pre-train a ViT backbone through a double-stream architecture according to the PIM objective described in Sec. 3. Moreover, we consider the standard BEiT model [1] (*i.e.*, a MIM-based pre-training with block-wise masking) and CAE [7]. The CAE method employs an encoder-decoder architecture where the encoder processes only visible image patches (50% of the entire image), while the remaining 50% is masked. A latent contextual regressor predicts the masked representation based on the encoder output, and a lightweight decoder processes the output of the regressor, which is then used to predict the visual token of the related masked patches.

**Image classification setup.** During the classification fine-tuning stage, the final hidden layer of the ViT-based backbone extracts features that are then combined via average pooling to generate a global image representation. This representation is subsequently fed into a softmax classifier. Following

Table 1: Fine-tuning results of different pre-training objectives in terms of top-1 and linear probe accuracy on ImageNet-1k. We report the results using both the VQ-KD and  $k$ -CLIP tokenizers.

Method	Tokenizer	ViT-T		ViT-S		ViT-B	
		Top-1 Acc. (%)	Linear Probe Acc. (%)	Top-1 Acc. (%)	Linear Probe Acc. (%)	Top-1 Acc. (%)	Linear Probe Acc. (%)
MIM	VQ-KD	74.6	55.3	82.0	<b>69.9</b>	83.8	72.3
<b>PIM</b>	VQ-KD	<b>74.9</b>	56.4	82.1	68.7	83.7	73.3
<b>MaPeT</b>	VQ-KD	74.5	<b>59.6</b>	<b>82.2</b>	69.8	<b>84.4</b>	<b>73.8</b>
MIM	$k$ -CLIP	74.9	60.4	82.0	71.1	83.3	72.3
<b>PIM</b>	$k$ -CLIP	75.3	59.7	81.8	69.5	83.3	<b>73.5</b>
<b>MaPeT</b>	$k$ -CLIP	<b>75.5</b>	<b>62.5</b>	<b>82.1</b>	<b>71.6</b>	<b>83.6</b>	<b>73.5</b>

Table 2: Fine-tuning results in comparison with existing self-supervised pre-training approaches, in terms of top-1 and linear probe accuracy on ImageNet-1k.

Method	Tokenizer	ViT-T		ViT-S		ViT-B	
		Top-1 Acc. (%)	Linear Probe Acc. (%)	Top-1 Acc. (%)	Linear Probe Acc. (%)	Top-1 Acc. (%)	Linear Probe Acc. (%)
ViT [14]	-	73.7	-	79.8	-	81.8	-
CAE [7]	VQ-KD	73.4	52.4	81.6	63.4	83.5	69.4
BEiT [1]	VQ-KD	<b>75.0</b>	<b>62.0</b>	<b>82.2</b>	<b>72.6</b>	<b>84.4</b>	<b>75.0</b>
<b>MaPeT</b>	VQ-KD	74.5	59.6	<b>82.2</b>	69.8	<b>84.4</b>	73.8
CAE [7]	$k$ -CLIP	73.7	53.9	81.5	62.9	82.7	67.6
BEiT [1]	$k$ -CLIP	74.8	61.5	81.9	71.1	83.3	73.3
<b>MaPeT</b>	$k$ -CLIP	<b>75.5</b>	<b>62.5</b>	<b>82.1</b>	<b>71.6</b>	<b>83.6</b>	<b>73.5</b>

the linear probing experiment reported in [1], we also train a linear classifier head over the output representation produced by the frozen pre-trained backbone.

We design three different model variants based on Vision Transformer [14], *i.e.*, ViT-Tiny (ViT-T), ViT-Small (ViT-S), and ViT-Base (ViT-B). Our MaPeT model is trained by setting the cutting point  $c$  to 50, 50, and 60, respectively. We refer the reader to the supplementary material for detailed pre-training and fine-tuning hyperparameters, and for an ablation analysis on cutting point values.

## 5.2 Experimental Results

**Pre-training objectives comparison.** To validate the assumptions made on the pre-training objectives presented in Section 4, we conduct a comparison of MIM, PIM, and our proposed MaPeT, as shown in Table 1. This comparison evaluates the top-1 accuracy and linear probe accuracy of these approaches. The results indicate that MIM pre-training is less effective compared to PIM due to the input noise introduced by masked tokens and the independent reconstruction of patches. PIM outperforms MIM in most comparisons. For instance, when employing ViT-T with  $k$ -CLIP and ViT-S with VQ-KD, PIM achieves improvements of 0.4% and 0.1% in classification accuracy, respectively, over MIM. However, PIM demonstrates comparable performance to MIM when applied to the ViT-B backbone. Furthermore, our proposed MaPeT consistently outperforms PIM in nearly all cases. It exhibits accuracy gains of 0.2%, 0.3%, and 0.7% in top-1 accuracy, as well as 2.8%, 2.1%, and 0.5% in linear probe accuracy respectively on ViT-T and ViT-S when using the  $k$ -CLIP tokenizer, and on ViT-B when employing the VQ-KD tokenizer. These findings underscore the significance of addressing position inconsistency between pre-training and fine-tuning, particularly in the context of permutation-based image pre-training.

**Comparison with state-of-the-art models.** Table 2 presents a comprehensive analysis of the performance of MaPeT, BEiT, and CAE in terms of top-1 accuracy and linear probe accuracy across all ViT-based backbones. Firstly, our pre-trained MaPeT model showcases significant performance improvements across all Tiny, Small, and Base backbones compared to ViT-based models trained with random initialization, as evidenced in Table 2. Secondly, our results demonstrate that both BEiT and MaPeT outperform CAE. We hypothesize that the CAE encoder, which only observes 50% of the total sequence during pre-training, may suffer from position discrepancies between the pre-training and fine-tuning phases. Thirdly, it is noteworthy that BEiT improves overall results

Table 3: Comparison with state-of-the-art self-supervised pre-training models in terms of top-1 accuracy on ImageNet-1k. Results of competitors are extracted from the original papers.

Method	# Epochs	ViT-S		ViT-B		
		Top-1 Acc. (%)	Top-1 Acc. (%)	Method	# Epochs	Top-1 Acc. (%)
BEiT [1]	300	81.7	82.9	BEiT [1]	800	83.2
CAE [7]	300	82.0	83.6	CAE [7]	800	83.8
SplitMask [15]	300	-	83.6	CAE [7]	1600	83.9
MaskFeat [35]	300	-	83.6	BEiT v2 [30]	1600	85.5
PeCo [13]	300	-	84.1			
MVP [36]	300	-	84.4			
BEiT v2 [30]	300	-	<b>85.0</b>			
<b>MaPeT (k-CLIP)</b>	300	<b>82.1</b>	<b>83.6</b>			
<b>MaPeT (VQ-KD)</b>	300	<b>82.2</b>	84.4			

compared to MIM in Table 1. We attribute this improvement to the blockwise masking technique employed by BEiT. This technique follows the principle of image spatial locality, which posits that adjacent patches exhibit similarities in terms of visual information. By employing blockwise masking, the density of uncorrupted visual content is increased, while the noise introduced by masked tokens is concentrated in fewer locations instead of being sparsely distributed. Furthermore, MaPeT consistently outperforms all competitors across the three model variants when employing the  $k$ -CLIP tokenizer. Specifically, our model achieves top-1 accuracy margins of 0.7%, 0.2%, and 0.3% against BEiT on ViT-T, ViT-S, and ViT-B, respectively, while exhibiting margins of 1.8%, 0.6%, and 0.9% against CAE across the same three backbones. In contrast, MaPeT demonstrates comparable results to BEiT when employing the VQ-KD tokenizer on the ViT-S and ViT-B backbones.

We also report the comparison of our best variants and other state-of-the-art self-supervised pre-training models in Table 3. Note that the variability in the experimental settings and the different supervisory signals used in each approach may affect the fairness of the comparisons. Notably, although current literature has not extensively explored performance benchmarking on the ViT-S backbone, the Small version of our MaPeT model outperforms BEiT [1] and CAE [7] by 0.5% and 0.2% respectively, yielding the best performance for both  $k$ -CLIP and VQ-KD. In the case of the ViT-B backbone, MaPeT surpasses the majority of the considered approaches especially when using the VQ-KD tokenizer, except for BEiT v2 [30] which gets slightly better results. This performance gap can be explained by the lack of data augmentation in our model pre-training, which can significantly increase performance but at a higher computational cost.

All the results presented in Table 3 are obtained after pre-training the models for 300 epochs. For completeness, on the right side, we report the performance of other methods when pre-trained for a considerably large number of epochs (*i.e.*, 800 and 1600). While a direct comparison using different pre-training epochs may not be completely informative, MaPeT still proves to perform better than other methods pre-trained for a larger number of epochs such as BEiT and CAE.

### 5.3 Visual Tokenizer Analysis

In this section, we present a comprehensive qualitative and quantitative analysis of our proposed  $k$ -CLIP and compare its performance to the existing DALL-E [32] and VQ-KD [30] tokenizers.

**Impact of tokenizer on model performance.** Analyzing the results in Table 1, it can be noted that  $k$ -CLIP outperforms VQ-KD across all models evaluated on ViT-T, with improvements in top-1 accuracy of 1.0%, 0.4%, and 0.3% observed on MaPeT, PIM, and MIM, respectively. However, the results differ when evaluated on ViT-S and ViT-B, where VQ-KD exhibits better classification performance. We argue that the simpler semantic features of  $k$ -CLIP, with their inherent correlation with the semantic density of the image, can serve as a more effective self-supervisory signal for smaller models. On the other hand, the VQ-KD codebook is trained specifically to reconstruct CLIP features, making it a more demanding pre-training signal and thus more suitable for larger models.

**Image classification with discrete visual tokens.** In this section, we analyze image classification performance when using discretized visual tokens directly as input to the model. We conduct this analysis using the previously employed tokenizers (*i.e.*, our  $k$ -CLIP and VQ-KD [30]) and also include the DALL-E visual tokenizer [32], which consists of a discrete variational autoencoder model. Specifically, we map the sequence of visual tokens to an embedding space of dimension  $D$  through

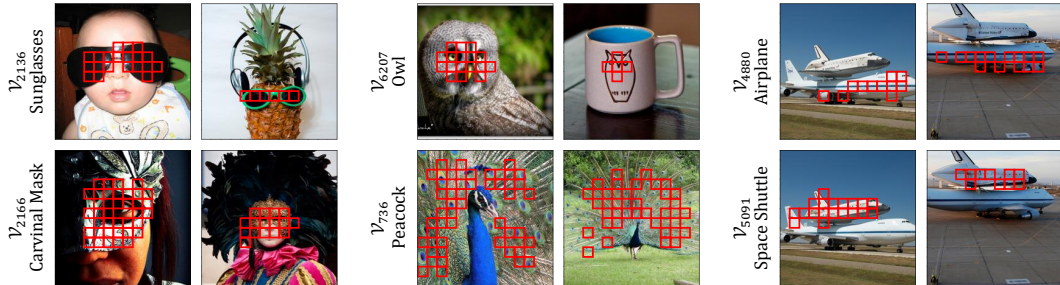


Figure 3: Visualization of image patches corresponding to the discrete tokens of our  $k$ -CLIP codebook, where semantically similar patches consistently share the same discrete token.

Table 4: Accuracy of image classification when employing visual tokens as model input. Note that using CLIP features for zero-shot image classification leads to a top-1 accuracy of 73.6%.

Tokenizer	MLP		ViT-T	
	Top-1 Acc. (%)	Top-5 Acc. (%)	Top-1 Acc. (%)	Top-5 Acc. (%)
DALL-E	4.1	11.7	9.1	21.9
VQ-KD	68.1	89.8	72.3	92.2
<b>k-CLIP</b>	<b>72.8</b>	<b>93.2</b>	<b>76.2</b>	<b>94.9</b>

learnable embeddings trained in conjunction with two different model backbones: a lightweight MLP classification head and a ViT-Tiny model. The MLP head comprises an embedding layer, a linear layer with output dimension  $D = 192$ , a ReLU activation, an average pooling operation, and an additional linear layer that projects the pooled features to the number of classes (*i.e.*, 1000).

The results shown in Table 4 indicate that the use of DALL-E visual tokens yields limited accuracy in this setting. This can be attributed to the relatively low amount of semantic information derived from the reconstruction task that DALL-E is trained on. In contrast,  $k$ -CLIP demonstrates significant performance superiority over alternative tokenizers when employed with both the MLP head and ViT-Tiny backbone. This observed trend can be attributed to the rich semantic information inherent in CLIP visual features, which is effectively preserved through the process of  $k$ -means discretization. Consequently, a strong correlation between visual tokens and image classes can be established, leading to favorable performance outcomes even when utilizing small models such as the MLP head.

**Codebook visualization.** Fig. 3 presents a collection of examples that showcase the semantic associations between image patches and visual tokens, extracted using our  $k$ -CLIP tokenizer. This visualization effectively demonstrates the efficacy of our tokenizer in accurately capturing and representing the semantic content of the images within the considered dataset and shows its ability to recognize and group image patches that share common visual features and semantic meaning. As it can be noticed, the visual tokens shown are congruent with specific semantic concepts, albeit resulting in distinct representations for similar visual elements such as sunglasses and carnival mask, owl and peacock, or airplane and space shuttle. Furthermore, it is worth noting that the visual tokens remain resilient to variations in color, style, rotation, and size. This is exemplified by the middle example, where the image depicts an owl print on a cup, yet it is still accurately identified using the owl visual token. These observations emphasize the ability of our  $k$ -CLIP tokenizer to effectively identify and classify complex visual concepts.

## 6 Conclusion

This paper presents MaPeT, a novel self-supervised pre-training approach designed for vision tasks. Our model effectively tackles the limitations of standard Masked Image Modeling, employing a permutation-based objective to capture the interdependencies among predicted tokens and auxiliary position information to enable the model to access a full sequence of image patches. Moreover, we introduce the  $k$ -CLIP tokenizer that can densely capture the semantic information of the visual input by leveraging discretized CLIP features as visual tokens. Experimental results demonstrate that our approach achieves improved fine-tuning performance on image classification, outperforming direct competitors under the same experimental setting.

## Acknowledgments and Disclosure of Funding

We thank CINECA for providing computational resources. This work has partially been supported by the projects PNRR-M4C2 (PE00000013) “FAIR - Future Artificial Intelligence Research” funded by the European Commission and “ELSA - European Lighthouse on Secure and Safe AI” funded by the EU (GA 101070617).

## Supplementary Material

In the following, we explore the adaptability of our model to novel data domains and examine the influence of varying the reconstruction factor on the performance of the model. Furthermore, we provide additional qualitative visualizations of the codebook associated with the proposed  $k$ -CLIP tokenizer, supplementary implementation details, and a discussion on the potential limitations and social implications of the proposed methodology.

## A Cross-Domain Transfer Learning Capabilities

In this section, we examine the generalization capabilities of our proposed self-supervised pre-training technique, in comparison to BEiT [1] and CAE [7]. All the considered architectures employ the VQ-KD visual tokenizer [30] and undergo pre-training on the extensive ImageNet-1k dataset [10]. Subsequently, they are fine-tuned on three distinct data domains, namely Stanford-Cars [23], Food-101 [2], and FGVC-Aircraft [27]. These datasets are chosen to represent diverse and real-world scenarios, ranging from object recognition in the automotive domain to food and aircraft classification. By employing a linear probe evaluation, we can quantitatively measure the ability of our pre-trained model to transfer knowledge and adapt to new tasks without fine-tuning.

The results, presented in Table 5, clearly demonstrate the superior performance of our MaPeT model across all considered datasets. Our model outperforms both BEiT and CAE, highlighting its robustness and efficacy in capturing meaningful visual representations.

These findings not only underline the potential of MaPeT as a powerful pre-training technique but also emphasize its cross-domain transfer learning capabilities, which enable practical relevance in various real-world applications.

## B Reconstruction Ratio Analysis

Here we discuss the relationship between the reconstruction ratio employed in the MaPeT model and its impact on image classification performance. The reconstruction ratio indicates the proportion of target patches in relation to the entire input sequence.

An advantage of MaPeT is that it attends to the target patch  $x_{z_t} \in x_{z>c}$  during the prediction of  $x_{z_{t+1}}$ , allowing for the cutting point  $c$  to be positioned at every value in the interval  $c \in [1 \dots N - 1]$ . This unique feature of MaPeT enables the potential reconstruction of all patches in an incremental and randomized manner, from the first to the last patch. On the other hand, the BEiT and CAE models lack the ability to reconstruct all image patches because doing so would lead to a masking ratio that is too high, resulting in the loss of visual context necessary for the reconstruction of the masked elements. Table 6 refers to the analysis of the reconstruction ratio on the ViT-B architecture. It can be noted that MaPeT exhibits a preference for a reconstruction ratio of approximately 70% of the complete sequence. Indeed, the initial target patches are compelled to establish correlations with a small portion of visible patches (namely, 30% of the entire sequence) randomly distributed throughout the image.

The model can acquire long-range spatial dependencies that are contingent on the position of the target patch in the permuted order. As the final patches attend to the majority of the visual content, they are likely to concentrate more on neighboring image patches, consistent with the principle of spatial locality. A reduction in the reconstruction ratio leads to an increase in the number of visible patches attended by the target patches that occur early in the permuted order. This results in an increase in the likelihood of having neighboring visible patches, which, in turn, diminishes the learned long-range spatial dependencies. In contrast, an excessively high reconstruction ratio of 85% makes

Table 5: Comparison of model performance on cross-domain transfer learning. We measure the linear probe accuracy of our proposed MaPeT model compared to BEiT and CAE on three distinct data domains: Stanford-Cars, Food-101, and FGVC-Aircraft.

Method	Tokenizer	Linear Probe Acc. (%)		
		Stanford-Cars [23]	Food-101 [2]	FGVC-Aircraft [27]
CAE [7]	VQ-KD	53.6	81.4	40.5
BEiT [1]	VQ-KD	64.5	<b>86.9</b>	44.9
<b>MaPeT</b>	VQ-KD	<b>68.5</b>	<b>86.9</b>	<b>46.8</b>

Table 6: Ablation study on the impact of the reconstruction factor (%) on the top-1 fine-tuning accuracy of pre-trained ViT-B under the VQ-KD setting.

Cutting point $c$	Reconstruction ratio	Tokenizer	Top-1 Accuracy (%)
30	85%	VQ-KD	84.2
40	80%	VQ-KD	84.3
50	75%	VQ-KD	84.3
60	70%	VQ-KD	<b>84.4</b>
98	50%	VQ-KD	84.1

the pre-training objective of MaPeT excessively difficult, as early predictions are likely to be arbitrary, having access to only 15% of the overall visual information. Consequently, excessively high or low reconstruction ratios impair the performance, as evidenced by Table 6.

These observations shed light on the interplay between the reconstruction ratio and the capacity of the model to capture spatial relationships. The optimal reconstruction ratio, as evidenced by our findings, strikes a balance between capturing long-range dependencies and leveraging the spatial locality inherent in the visual data.

## C Additional Codebook Visualization

In Figure 4 we report a supplementary compilation of examples previously introduced in Subsection 5.3. Within this collection, distinct visual tokens successfully represent semantic concepts. Notably, the pairs of Clownfish and Lionfish, Leopard snout and Cougar snout, Yellow butterfly and Yellow flower, as well as Bicycle and Unicycle, further validate the discriminative nature of visual tokens, even for highly similar categories.

In Figure 5, we also show some examples of image patches that mismatch the semantic concepts associated with the discrete tokens of the codebook. Indeed, we observe some incongruities that may be linked to the resemblance of patches to other semantic concepts. For instance, in the first row of the figure, some image patches are identified with the Peacock visual tokens while the bird species are different. The sumptuous tails of these birds can be visually associated with the characteristic features of a peacock. Similarly, in the second row of the image, the silver and gold perforations, which are associated with medieval headgear or adornments, may be perceived as comparable to the reflective surface of a carnival mask. Furthermore, within the third row of the figure, it is worth noting that several images do not precisely match the semantically correct concept of Space Shuttle. Nevertheless, these images demonstrate a semantic affinity with the broader, higher-level concept of “Space”. The images contain a variety of visual elements, including the NASA logo, astronauts, planets, and even aliens. While the specific content of these images may diverge from the targeted concept, the overall semantic theme they evoke can be seen as related to the broader concept of space exploration and travel. These observations highlight our  $k$ -CLIP tokenizer enables the identification and classification of complex visual concepts.

## D Additional Implementation Details

**Hyperparameters for Pre-Training.** In Table 7, we schematize the experimental settings adopted during the pre-training phase.

**Hyperparameters for Fine-Tuning.** The complete experimental configuration for fine-tuning our classification models is outlined in Table 8.

**Hyperparameters for Linear Probe.** Linear probing has been a widely considered proxy for assessing the effectiveness of self-supervised pre-training models. In accordance with the approach outlined in [1], we train a linear classifier head over the image-level representation output produced by the frozen pre-trained backbone. We use the class labels of the images to train the aforementioned classifier head. We train for 50 epochs using a batch size of 1024, AdamW [26] as optimizer, and a learning rate of  $4e-3$  with cosine decay. The weight decay is set to  $1e-4$ . Our pre-training augmentation strategy incorporates random resizing of crops, horizontal flipping during training, and central crops during evaluation.

**Computational Requirements.** The pre-training experiments conducted with our MaPeT model involved the utilization of different GPU configurations. Specifically, the ViT-T, ViT-S, and ViT-B models required the deployment of 16, 32, and 64 GPUs, respectively. The pre-training process for each model took approximately one day to complete. In contrast, during the fine-tuning phase, we employed 4 GPUs for the ViT-T and ViT-S models, and 16 GPUs for the ViT-B model. The fine-tuning duration for each model was 48 hours, 36 hours, and 12 hours, respectively. For all experiments, we utilized the NVIDIA V100 GPU architecture, which was equipped with 16GB of memory and ran on IBM POWER9 AC922 CPUs operating at 3.1 GHz.

## E Limitations and Societal Impact

The findings presented in Sec. A highlight the potential of MaPeT as a powerful pre-training technique for various real-world applications. The ability of MaPeT to effectively transfer knowledge across different domains opens up opportunities for more efficient and accurate visual recognition systems. By reducing the reliance on domain-specific labeled data, MaPeT offers a promising avenue for addressing the data scarcity challenge in various domains. However, it is important to acknowledge certain limitations and challenges associated with our study. MaPeT necessitates significant computational resources at training time, which can be demanding in terms of both hardware and time. These computational requirements of MaPeT can pose challenges for its widespread adoption and practical implementation, particularly in settings with limited access to high-end computing resources. While the performance benefits of MaPeT have been demonstrated in the evaluated datasets, it is important to consider the scalability and adaptability of the proposed method to even more diverse and complex domains.

## References

- [1] Hangbo Bao, Li Dong, Songhao Piao, and Furu Wei. BEiT: BERT pre-training of image Transformers. In *ICLR*, 2022.
- [2] Lukas Bossard, Matthieu Guillaumin, and Luc Van Gool. Food-101—mining discriminative components with random forests. In *ECCV*, 2014.
- [3] Tom Brown, Benjamin Mann, Nick Ryder, Melanie Subbiah, Jared D Kaplan, Prafulla Dhariwal, Arvind Neelakantan, Pranav Shyam, Girish Sastry, Amanda Askell, Sandhini Agarwal, Ariel Herbert-Voss, Gretchen Krueger, Tom Henighan, Rewon Child, Aditya Ramesh, Daniel Ziegler, Jeffrey Wu, Clemens Winter, Chris Hesse, Mark Chen, Eric Sigler, Mateusz Litwin, Scott Gray, Benjamin Chess, Jack Clark, Christopher Berner, Sam McCandlish, Alec Radford, Ilya Sutskever, and Dario Amodei. Language models are few-shot learners. *NeurIPS*, 2020.
- [4] Mathilde Caron, Hugo Touvron, Ishan Misra, Hervé Jégou, Julien Mairal, Piotr Bojanowski, and Armand Joulin. Emerging properties in self-supervised vision transformers. In *ICCV*, 2021.
- [5] Mark Chen, Alec Radford, Rewon Child, Jeffrey Wu, Heewoo Jun, David Luan, and Ilya Sutskever. Generative Pretraining From Pixels. In *ICML*, 2020.
- [6] Ting Chen, Simon Kornblith, Mohammad Norouzi, and Geoffrey Hinton. A simple framework for contrastive learning of visual representations. In *ICML*, 2020.
- [7] Xiaokang Chen, Mingyu Ding, Xiaodi Wang, Ying Xin, Shentong Mo, Yunhao Wang, Shumin Han, Ping Luo, Gang Zeng, and Jingdong Wang. Context Autoencoder for Self-Supervised Representation Learning. *arXiv preprint arXiv:2202.03026*, 2022.

Table 7: Hyperparameters for pre-training on ImageNet-1k [10].

Hyperparameter	Tiny Size	Small Size	Base Size
Hidden size	192	384	768
FFN inner hidden size	768	1536	3072
Attention heads	3	6	12
Layers		12	
Attention head size		64	
Layer scale		0.1	
Patch size		16 × 16	
Training epochs		300	
Batch size		2048	
Optimizer		AdamW	
Adam $\epsilon$		1e-8	
Adam $\beta$		(0.9, 0.999)	
Peak learning rate		1.5e-3	
Minimal learning rate		1e-5	
Warmup learning rate		1e-6	
Learning rate schedule		Cosine	
Warmup epochs		10	
Gradient clipping		3.0	
Dropout		$\times$	
Stoch. depth		0.1	
Weight decay		0.05	
Input resolution		224 × 224	
Color jitter		0.4	

Table 8: Hyperparameters for fine-tuning on ImageNet-1k [10].

Hyperparameter	Tiny Size	Small Size	Base Size
Peak learning rate	2.5e-4	5e-3	5e-4
Fine-tuning epochs	300	200	100
Layer-wise learning rate decay	$\times$	0.65	0.65
Batch size		1024	
Warmup epochs		20	
Optimizer		AdamW	
Adam $\epsilon$		1e-8	
Adam $\beta$		(0.9, 0.999)	
Minimal learning rate		1e-6	
Warmup learning rate		1e-6	
Learning rate schedule		Cosine	
Weight decay		0.05	
Label smoothing $\epsilon$		0.1	
Stoch. depth		0.1	
Dropout		$\times$	
Gradient clipping		$\times$	
Erasing prob.		0.25	
Input resolution		224 × 224	
Rand Augment		9/0.5	
Mixup prob.		0.8	
Cutmix prob.		1.0	

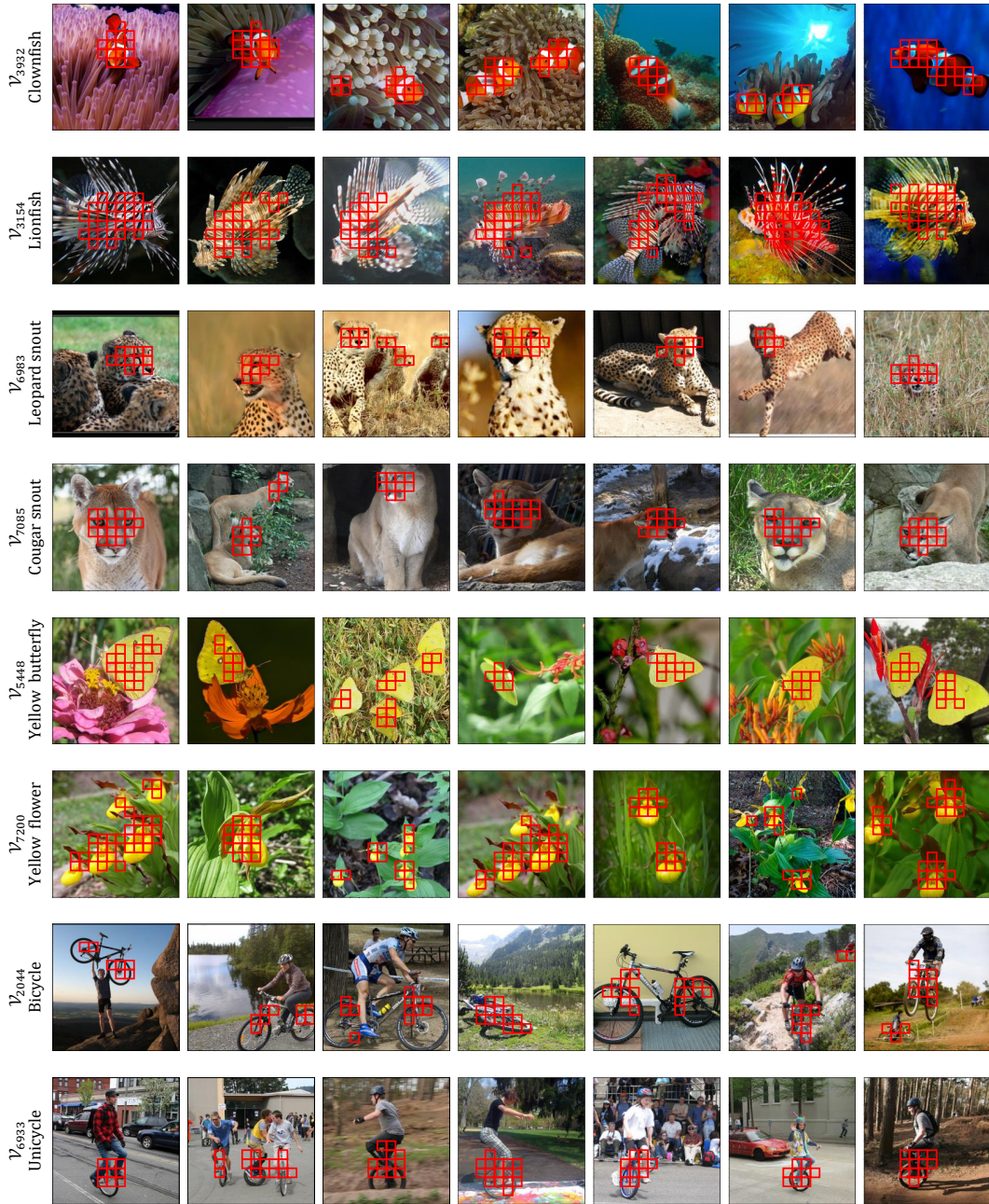


Figure 4: Visualization of image patches corresponding to the discrete tokens contained within our  $k$ -CLIP codebook. The codebook exhibits a high degree of semantic density and coherency, *i.e.*, semantically similar image patches are consistently linked with the same discrete token in the visual codebook. Corresponding image patches are marked in red rectangle.

- [8] Xinlei Chen and Kaiming He. Exploring simple siamese representation learning. In *CVPR*, 2021.
- [9] Xinlei Chen, Saining Xie, and Kaiming He. An empirical study of training self-supervised vision transformers. In *ICCV*, 2021.
- [10] Jia Deng, Wei Dong, Richard Socher, Li-Jia Li, Kai Li, and Li Fei-Fei. ImageNet: A large-scale hierarchical image database. In *CVPR*, 2009.
- [11] Jacob Devlin, Ming-Wei Chang, Kenton Lee, and Kristina Toutanova. BERT: Pre-training of Deep Bidirectional Transformers for Language Understanding. In *NAACL*, 2019.

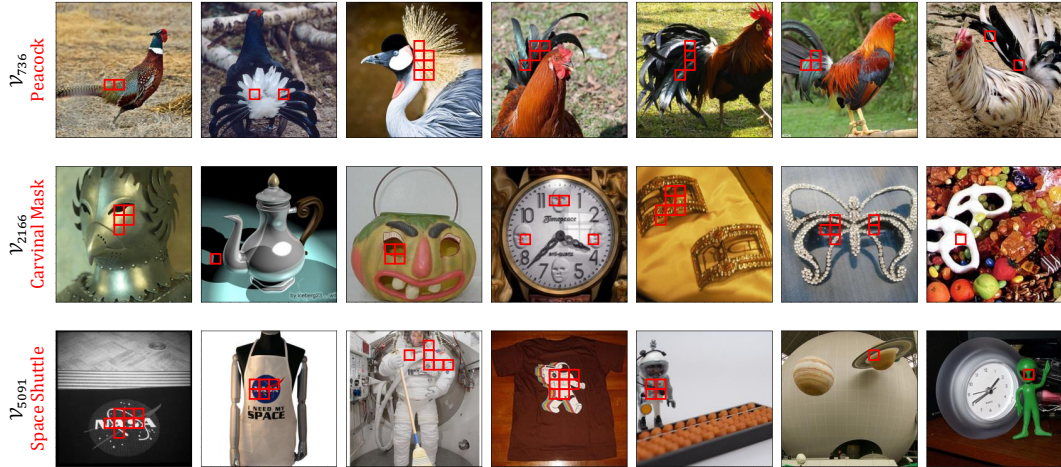


Figure 5: Visualization of image patches mismatching the semantic concept associated with the discrete tokens contained within our  $k$ -CLIP codebook. Corresponding image patches are marked in red rectangle.

- [12] Carl Doersch, Abhinav Gupta, and Alexei A Efros. Unsupervised Visual Representation Learning by Context Prediction. In *ICCV*, 2015.
- [13] Xiaoyi Dong, Jianmin Bao, Ting Zhang, Dongdong Chen, Weiming Zhang, Lu Yuan, Dong Chen, Fang Wen, and Nenghai Yu. PeCo: Perceptual Codebook for BERT Pre-training of Vision Transformers. In *AAAI*, 2023.
- [14] Alexey Dosovitskiy, Lucas Beyer, Alexander Kolesnikov, Dirk Weissenborn, Xiaohua Zhai, Thomas Unterthiner, Mostafa Dehghani, Matthias Minderer, Georg Heigold, Sylvain Gelly, Jakob Uszkoreit, and Neil Houlsby. An Image is Worth 16x16 Words: Transformers for Image Recognition at Scale. In *ICLR*, 2021.
- [15] Alaaeldin El-Nouby, Gautier Izacard, Hugo Touvron, Ivan Laptev, Hervé Jegou, and Edouard Grave. Are Large-scale Datasets Necessary for Self-Supervised Pre-training? *arXiv preprint arXiv:2112.10740*, 2021.
- [16] Yuxin Fang, Li Dong, Hangbo Bao, Xinggang Wang, and Furu Wei. Corrupted image modeling for self-supervised visual pre-training. *arXiv preprint arXiv:2202.03382*, 2022.
- [17] Spyros Gidaris, Praveer Singh, and Nikos Komodakis. Unsupervised representation learning by predicting image rotations. In *ICLR*, 2018.
- [18] Jean-Bastien Grill, Florian Strub, Florent Altché, Corentin Tallec, Pierre Richemond, Elena Buchatskaya, Carl Doersch, Bernardo Avila Pires, Zhaohan Guo, Mohammad Gheshlaghi Azar, Bilal Piot, Koray Kavukcuoglu, Remi Munos, and Michal Valko. Bootstrap your own latent-a new approach to self-supervised learning. *NeurIPS*, 2020.
- [19] Kaiming He, Xinlei Chen, Saining Xie, Yanghao Li, Piotr Dollár, and Ross Girshick. Masked Autoencoders Are Scalable Vision Learners. In *CVPR*, 2022.
- [20] Kaiming He, Haoqi Fan, Yuxin Wu, Saining Xie, and Ross Girshick. Momentum contrast for unsupervised visual representation learning. In *CVPR*, 2020.
- [21] Zejiang Hou, Fei Sun, Yen-Kuang Chen, Yuan Xie, and Sun-Yuan Kung. MILAN: Masked Image Pretraining on Language Assisted Representation. *arXiv preprint arXiv:2208.06049*, 2022.
- [22] Zhicheng Huang, Xiaojie Jin, Chengze Lu, Qibin Hou, Ming-Ming Cheng, Dongmei Fu, Xiaohui Shen, and Jiashi Feng. Contrastive masked autoencoders are stronger vision learners. *arXiv preprint arXiv:2207.13532*, 2022.
- [23] Jonathan Krause, Michael Stark, Jia Deng, and Li Fei-Fei. 3d object representations for fine-grained categorization. In *ICCV*, 2013.
- [24] Yinhan Liu, Myle Ott, Naman Goyal, Jingfei Du, Mandar Joshi, Danqi Chen, Omer Levy, Mike Lewis, Luke Zettlemoyer, and Veselin Stoyanov. RoBERTa: A Robustly Optimized BERT Pretraining Approach. *arXiv preprint arXiv:1907.11692*, 2019.

- [25] Ze Liu, Han Hu, Yutong Lin, Zhuliang Yao, Zhenda Xie, Yixuan Wei, Jia Ning, Yue Cao, Zheng Zhang, Li Dong, et al. Swin Transformer V2: Scaling Up Capacity and Resolution. In *CVPR*, 2022.
- [26] Ilya Loshchilov and Frank Hutter. Decoupled weight decay regularization. In *ICLR*, 2019.
- [27] S. Maji, J. Kannala, E. Rahtu, M. Blaschko, and A. Vedaldi. Fine-grained visual classification of aircraft. Technical report, 2013.
- [28] Mehdi Noroozi and Paolo Favaro. Unsupervised Learning of Visual Representations by Solving Jigsaw Puzzles. In *ECCV*, 2016.
- [29] Aaron van den Oord, Yazhe Li, and Oriol Vinyals. Representation learning with contrastive predictive coding. *arXiv preprint arXiv:1807.03748*, 2018.
- [30] Zhiliang Peng, Li Dong, Hangbo Bao, Qixiang Ye, and Furu Wei. BEiT v2: Masked Image Modeling with Vector-Quantized Visual Tokenizers. *arXiv preprint arXiv:2208.06366*, 2022.
- [31] Alec Radford, Jong Wook Kim, Chris Hallacy, Aditya Ramesh, Gabriel Goh, Sandhini Agarwal, Girish Sastry, Amanda Askell, Pamela Mishkin, Jack Clark, Gretchen Krueger, and Ilya Sutskever. Learning transferable visual models from natural language supervision. In *ICML*, 2021.
- [32] Aditya Ramesh, Mikhail Pavlov, Gabriel Goh, Scott Gray, Chelsea Voss, Alec Radford, Mark Chen, and Ilya Sutskever. Zero-Shot Text-to-Image Generation. In *ICML*, 2021.
- [33] Kaitao Song, Xu Tan, Tao Qin, Jianfeng Lu, and Tie-Yan Liu. MPNet: Masked and Permuted Pre-training for Language Understanding. *NeurIPS*, 2020.
- [34] Xiaolong Wang and Abhinav Gupta. Unsupervised learning of visual representations using videos. In *ICCV*, 2015.
- [35] Chen Wei, Haoqi Fan, Saining Xie, Chao-Yuan Wu, Alan Yuille, and Christoph Feichtenhofer. Masked feature prediction for self-supervised visual pre-training. In *CVPR*, 2022.
- [36] Longhui Wei, Lingxi Xie, Wengang Zhou, Houqiang Li, and Qi Tian. MVP: Multimodality-guided Visual Pre-training. In *ECCV*, 2022.
- [37] Zhenda Xie, Zheng Zhang, Yue Cao, Yutong Lin, Jianmin Bao, Zhuliang Yao, Qi Dai, and Han Hu. SimMIM: a Simple Framework for Masked Image Modeling. In *CVPR*, 2022.
- [38] Zhilin Yang, Zihang Dai, Yiming Yang, Jaime Carbonell, Russ R Salakhutdinov, and Quoc V Le. XLNet: Generalized Autoregressive Pretraining for Language Understanding. *NeurIPS*, 2019.
- [39] Richard Zhang, Phillip Isola, and Alexei A Efros. Colorful image colorization. In *ECCV*, 2016.
- [40] Xinyu Zhang, Jiahui Chen, Junkun Yuan, Qiang Chen, Jian Wang, Xiaodi Wang, Shumin Han, Xiaokang Chen, Jimin Pi, Kun Yao, Junyu Han, Errui Ding, and Jingdong Wang. CAE v2: Context Autoencoder with CLIP Target. *arXiv preprint arXiv:2211.09799*, 2022.